separations

MDPI

Article

On the Identification of Mobile and Stationary Zone Mass Transfer Resistances in Chromatography

Alessandra Adrover [1,*] and Gert Desmet [2]

[1] Department of Chemical Engineering, Materials, and Environment, Sapienza University of Rome, 00184 Rome, Italy
[2] Department of Chemical Engineering, Vrije Universiteit Brussel, 1050 Brussels, Belgium; gert.desmet@vub.be
* Correspondence: alessandra.adrover@uniroma1.it

Abstract: A robust and elegant approach, based on the Two-Zone Moment Analysis (TZMA) method, is proposed to assess the contributions of the mobile and stationary zones, H_{Cm} and H_{Cs}, to the C term H_C in the van Deemter equation for plate height. The TZMA method yields two formulations for H_{Cm} and H_{Cs}, both fully equivalent in terms of H_C, yet offering different decompositions of the contributions from the mobile and stationary zones. The first formulation proposes an expression for the term H_{Cs} that has strong similarities, but also significant differences, from the well-known and widely used one proposed by Giddings. While it addresses the inherent limitation of Giddings' approach—namely, the complete decoupling of transport phenomena in the moving and stationary zones—it introduces the drawback of a non-unique decomposition of H_C. Despite this, it proves highly valuable in highlighting the limitations and flaws of Giddings' method. In contrast, the second formulation not only properly accounts for the interaction between the moving and stationary zones, but provides a unique and consistent decomposition of H_C into its components. Three different geometries are investigated in detail: the 2D triangular array of cylinders (pillar array columns), the 2D array of rectangular pillars (radially elongated pillar array columns) and the 3D face-centered cubic array of spheres. It is shown that Giddings' approach significantly underestimates the H_{Cs} term, especially for porous-shell particles. Its accuracy is limited, being reliable only when intra-particle diffusivity (D_s) and the zone retention factor (k'') are very low, or when axially invariant systems are considered.

Keywords: liquid chromatography; band broadening; van Deemter equation; dispersion theory; hierarchical retentive porous media

check for updates

Academic Editor: Victoria Samanidou

Received: 31 January 2025
Revised: 20 February 2025
Accepted: 26 February 2025
Published: 28 February 2025

Citation: Adrover, A.; Desmet, G. On the Identification of Mobile and Stationary Zone Mass Transfer Resistances in Chromatography. *Separations* **2025**, *12*, 59. https://doi.org/10.3390/separations12030059

Copyright: © 2025 by the authors. Licensee MDPI, Basel, Switzerland. This article is an open access article distributed under the terms and conditions of the Creative Commons Attribution (CC BY) license (https://creativecommons.org/licenses/by/4.0/).

1. Introduction

Accurate models for band broadening are crucial for advancing the design of new stationary-phase materials and chromatographic columns, including 3D printed [1–3] and microfabricated pillar array columns [4–6]. In the context of particulate and monolithic materials, the General Plate Height Model (GPHM) is widely recognized [7,8] as the most reliable and widely accepted method for describing band broadening. According to the GPHM, the plate height H can be decomposed into four contributions:

$$H = \frac{2D^x}{U^x} = H_A + H_B + \underbrace{H_{Cm} + H_{Cs}}_{H_C} \tag{1}$$

where the first term H_A is associated with packing disorder, the second term H_B relates to longitudinal diffusion, while the third H_{Cm} and fourth H_{Cs} terms account for mass transfer resistances in the mobile and stationary zones, respectively. The total plate height H can be experimentally and numerically evaluated from the axial dispersion coefficient D^x and the effective axial velocity U^x along the main fluid flow direction x. For ordered packings, such as the arrays of spheres and pillar array columns, H_A is assumed to be negligible. The second term, H_B, also refereed to as the B term band broadening [9]

$$H_B = \frac{2D^{\text{eff}}}{U^x} \tag{2}$$

can be experimentally and numerically evaluated from peak parking experiments [10–12], allowing for the estimate of the longitudinal effective diffusion coefficient D^{eff}, or equivalently the obstruction factor $\gamma_m^0 = D^{\text{eff}}/D_m$, with D_m being the bare diffusion coefficient of the analyte in the elution solvent. Indeed, D^{eff} is the axial dispersion coefficient when the eluent flow is switched off, i.e., $D^{\text{eff}} = D^x|_{\mathbf{v}=\mathbf{0}}$. Numerous reliable models exist in the literature [13–16] to express the B term as a function of the geometric parameters of the porous medium and the zone retention factor k''. As far as it concerns the H_C term, the most common approach [7,8] is to assume that mass transfer in the mobile and stationary zone are actually two independent processes so that the H_{Cs} term, according to Giddings' non-equilibrium theory [17], can be simply expressed as

$$H_{Cs} = \frac{q_f}{4}\frac{k''}{(1+k'')^2}\frac{d_p^2}{D_s}U_i \tag{3}$$

where U_i is the interstitial velocity, d_p is the particle/pillar diameter, D_s is the diffusion coefficient in the meso-porous stationary zone and q_f is a shape factor depending exclusively on the geometry of the stationary zone. Equation (3) for the H_{Cs} term is fully equivalent to that obtained by the General Rate (GR) model [18] and the Parallel Zone model (PZ), as clearly discussed in [7]. By considering that H and H_B can be experimentally or numerically evaluated, and adopting Equation (3) for H_{Cs}, the mobile zone contribution H_{Cm} can be isolated [19–23]

$$H_{Cm} = H_C - H_{Cs} = (H - H_B) - H_{Cs} \tag{4}$$

and subsequently modelled via the GR or the PZ approaches as

$$H_{Cm} = \frac{2}{6}\frac{k''^2}{(1+k'')^2}\frac{d_p}{Sh_m}\left(\frac{U_i d_p}{D_m}\right) = \frac{2}{6}\frac{k''^2}{(1+k'')^2}\frac{d_p}{Sh_m}Pe \quad Sh_m = \text{Sherwood number} \tag{5}$$

or via more flexible expressions [21,22],

$$H_{Cm} = \frac{c_1 + c_2 k'' + c_3 k''^2}{(1+k'')^2}\frac{Pe}{f(Pe)} \tag{6}$$

or

$$H_{Cm} = \frac{f_1(Pe) + f_2(Pe)k'' + f_3(Pe)k''^2}{(1+k'')^2} \tag{7}$$

accounting for the nonlinear dependence of H_{Cm} on the Peclet number $Pe = U_i d_p/D_m$, also referred to as reduced velocity. It is therefore clear that all the models developed for the mobile H_{Cm} and stationary H_{Cs} mass transfer contributions are intrinsically based on the key assumption that mass transfers in the mobile and stationary zones are two independent processes, leading to Equations (3) and (4). However, this has already proven to be valid only for a few systems with relatively simple geometries, e.g., open-tubular liquid chromatography (OTLC) columns coated with a uniform meso-porous layer. Indeed,

Huygens et al. [21] clearly showed a failure of the additivity principle by analyzing dispersion data for 2D- and 3D-ordered periodic media, such as 2D arrays of cylinders and 3D arrays of spheres. Moreover, the need to take into account the strong interdependence between the mass transfer processes in the two zones has already been amply demonstrated by the theoretical models for D^{eff} [14–16], particularly in the simplest case where there is no convection affecting solute transport in the mobile zone.

The Two-Zone Moment Analysis (TZMA) method [24–26], recently proposed as a generalization of the classical Brenner moment approach to hierarchical porous media [27,28], allows us to accurately estimate the axial dispersion coefficient D^x in chromatographic systems with the further advantage that the final expression for D^x is formulated such that its terms are clearly associated with either the mobile or stationary zone. This framework provides a more direct understanding of the relative contributions of various band broadening phenomena in different parts of the system, their actual interdependence, as well as their dependence on analyte properties such as retention factor and diffusion coefficients. The objectives of the present work are threefold: (1) to propose a completely general method for identifying the terms H_{Cm} and H_{Cs} in periodic means based on the TZMA method; (2) to analyze, both analytically and numerically, the limits of applicability of the Giddings' approach; and (3) to quantify the error induced by the adoption of Equations (3) and (4) to the estimation of H_{Cm} and H_{Cs} for two-dimensional- and three-dimensional-ordered chromatographic systems such as cylindrical pillar arrays, elongated pillar arrays, and sphere arrays, all while varying the characteristic parameters such as the zone retention factor k'' and the ratio of diffusivities D_s/D_m in the two transport zones.

2. Materials and Methods

The Two-Zone Moment Analysis Approach

The TZMA approach allows us to model the transport of a single analyte through convection and diffusion within a fluid region Σ_m, in the presence of a meso-porous, adsorbing solid phase Σ_s. Let ε denote the external porosity of the chromatographic medium $\Sigma = \Sigma_m \cup \Sigma_s$. The solvent flow field $\mathbf{v}$, carrying the analyte under pressure-driven conditions, satisfies the Stokes equation with no-slip boundary conditions at the interface $\partial\Sigma_s$ between the mobile and stationary zones. Within the macro-porous fluid zone, solute transport occurs through both advective and diffusive processes, where D_m is the diffusion coefficient in the mobile zone. When the analyte enters the meso-porous solid zone, where no fluid motion is present, transport occurs solely via hindered diffusion in the meso-pores, subject to adsorption boundary conditions. Both effects are accounted for in the effective diffusion coefficient D_s, according to the General Rate model [25,29,30]. The meso-porous zone is characterized by the internal porosity ε_{int}, the specific surface area a [m^2/m^3], and the equilibrium adsorption constant K_{eq} [m], all of which are quantities contributing to the zone retention factor:

$$k'' = k_p \frac{V_s}{V_m} = \varepsilon_{\text{int}}(1 + K_{eq}a)\frac{V_s}{V_m} \tag{8}$$

where V_m is the volume occupied by the mobile fluid zone Σ_m, V_s the volume occupied by the stationary solid zone Σ_s (total particle volume, including the volume of the meso-pores), and k_p the partition coefficient related to the concentrations c_m and c_s in the mobile and stationary zones at the interface $\partial\Omega_s$, i.e., $c_m|_{\partial\Omega_s} = k_p c_s|_{\partial\Omega_s}$.

The TZMA approach shares two notable advantages with the Volume Averaging (VA) approach [29,30]. First, all calculations are performed within the single-unit lattice cell Ω, from whose spatial repetition the entire chromatographic medium Σ can be reproduced, i.e., $\Sigma = \cup_{i=1}^{N}\Omega_i$. Second, the transport equations only need to be solved for lower-order

moments in steady-state conditions. In contrast, Direct Numerical Simulations (DNSs) and Lattice Boltzmann (LB) methods [31–35] require solving the time-dependent advection-diffusion equation over a sufficiently large fluid domain, allowing chromatographic bands to reach asymptotic behavior, also referred to as macro-transport conditions [27].

Indeed, the TZMA method requires the solution of the following equations and boundary conditions for the stationary b-fields (so named after Brenner), namely the field b_m [m] defined in the mobile zone Ω_m, and the field b_s [m] defined in the stationary zone Ω_s:

$$D_m \nabla^2 b_m - \mathbf{v} \cdot \nabla b_m = (U^x - v_x) \tag{9}$$

$$D_s \nabla^2 b_s = U^x \tag{10}$$

$$b_m\big|_{\partial\Omega_s} = b_s\big|_{\partial\Omega_s} \tag{11}$$

$$-D_m(\nabla b_m - \mathbf{e}_x)\cdot\mathbf{n}\big|_{\partial\Omega_s} = k_p[-D_s(\nabla b_s - \mathbf{e}_x)\cdot\mathbf{n}]\big|_{\partial\Omega_s} \tag{12}$$

$$(\nabla b_s - \mathbf{e}_x)\cdot\mathbf{n}\big|_{\partial\Omega_s^{\text{imp}}} = 0 \tag{13}$$

where Ω_m and Ω_s are the mobile and stationary zones within the unit cell Ω, $\partial\Omega_s$ is the boundary between the two zones, $U^x = U_i/(1+k'')$ is the effective axial velocity, v_x is the axial velocity, $U_i = \langle v_x \rangle_{\Omega_m}$ is the interstitial axial velocity, $\mathbf{e}_x$ is the unit vector along x, and $\mathbf{n}$ is the normal vector pointing outward from the mobile zone. The boundary condition (13) applies if the stationary zone Ω_s is composed of a meso-porous zone and an impermeable core with boundary $\partial\Omega_s^{\text{imp}}$, as in the case of porous-shell particles or porous-shell pillars [13,22,36–38]. Furthermore, periodic boundary conditions are enforced at the edges of the unit cell Ω. The physical meaning of b_m and b_s is not so straightforward. The b-fields represent the stationary time-independent part of the first-order spatial moments of the analyte particles moving within the chromatography bed. For a detailed analysis of the method of moments and the derivation of b-fields, the reader is referred to [24,25,27].

The transport Equations (9) and (10) for b_m and b_s are independent of one another. However, b_m and b_s are intrinsically linked to each other through the boundary conditions (11) and (12). Numerical details on the solution of the transport equations for b_m and b_s by the Finite Element Method (FEM) are given in Appendix A.

From the b-fields, the total plate height H can be simply evaluated as

$$H = H_m + H_s = \underbrace{\frac{2D_m}{U_i}\left(1 - \langle \partial_x b_m \rangle_{\Omega_m}\right) + \frac{2}{U_i}\left\langle (v_x - U^x)\, b_m \right\rangle_{\Omega_m}}_{H_m} + \underbrace{\frac{2D_s k''}{U_i}\left(1 - \langle \partial_x b_s \rangle_{\Omega_s}\right) - \frac{2k'' U^x}{U_i}\left\langle b_s \right\rangle_{\Omega_s}}_{H_s} \tag{14}$$

or equivalently

$$H = H_m^g + H_s^g = \underbrace{\frac{2D_m}{U_i}\left\langle ||\nabla b_m - \mathbf{e}_x||^2 \right\rangle_{\Omega_m}}_{H_m^g} + \underbrace{\frac{2D_s\, k''}{U_i}\left\langle ||\nabla b_s - \mathbf{e}_x||^2 \right\rangle_{\Omega_s}}_{H_s^g} \tag{15}$$

where the symbols $\langle\cdot\rangle_{\Omega_m}$ and $\langle\cdot\rangle_{\Omega_s}$ indicate the spatial average over the mobile and stationary zone, respectively. Equations (14) and (15) are fully equivalent, meaning that they furnish exactly the same result in terms of H but allow for a different decomposition of the two contributions of the mobile and stationary zones. Indeed, it can be shown [25] that $H_m + H_s = H_m^g + H_s^g$ but $H_m \neq H_m^g$ and $H_s \neq H_s^g$.

3. Results and Discussion

3.1. Analysis of the b-Field b_s in the Stationary Zone

It must be observed that the b-fields b_m and b_s, solutions of the transport Equations (9)–(13) are defined up to an additive constant C that is the same for both fields. In other words, if b_m and b_s are solutions of Equations (9)–(13), then $b_m + C$ and $b_s + C$ are also solutions of the same transport scheme. Indeed, by replacing $b_m + C$ and $b_s + C$ into Equation (14) for H, an extra term appears, namely

$$\frac{2C\langle v_x - U^x\rangle_{\Omega_m}}{U_i} - \frac{2Ck''U^x}{U_i} = 2C\left(1 - \frac{1}{1+k''} - \frac{k''}{1+k''}\right) = 0$$

whose final value is zero $\forall k''$. Therefore, the value of the constant C is irrelevant to the evaluation of the total plate height H, but it affects the way the total H is partitioned into the two contributions H_m and H_s in Equation (14) because H_m and H_s depend explicitly on $\langle b_m\rangle_{\Omega_m}$ and $\langle b_s\rangle_{\Omega_s}$. On the contrary, H_m^g and H_s^g in Equation (15) are unaffected by the C value, as they depend exclusively on the gradients of the b-fields. This marks a profound difference between the two formulations, Equations (14) and (15), that aim to identify and separate the contribution of the moving zone from that of the stationary zone. By way of example, we analyzed the H_s term in a square array of fully porous cylinders (see Figure 1a) to see how it is influenced by the choice of the C constant. Setting the C constant corresponds to setting a specific value of b_m or b_s at one point on the boundary $\partial\Omega_s$. We analyzed three different cases, by setting $b_m = b_s = 0$ in point 1, 2 or 3, as shown in Figure 1a.

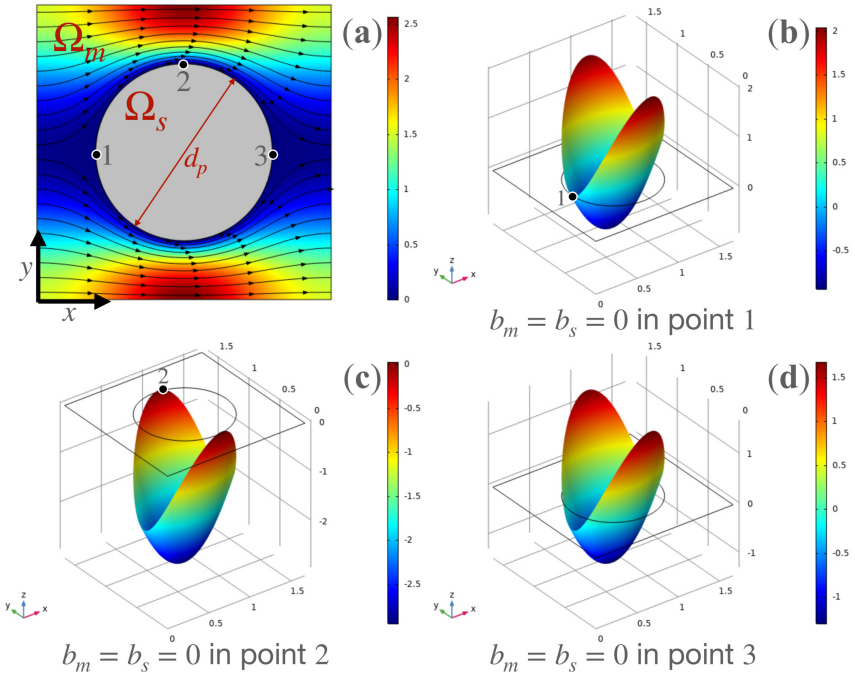


Figure 1. (**a**) Intensity I of the normalized velocity field $I = \sqrt{v_x^2 + v_y^2}/U_i$ and streamlines within the unit cell of the square array of fully porous cylinders. The figure highlights the fluid macro-porous region Ω_m, the meso-porous zone Ω_s (the stationary phase where adsorption takes place) and the three reference points. (**b**–**d**) Surface of the normalized b_s field b_s/d_p for $\alpha = D_s/D_m = 0.3$, $k'' = 4$ and $Pe = U_i d_p/D_m = 50$ in three different cases, namely $b_m = b_s = 0$ in point 1 (**b**), in point 2 (**c**), and in point 3 (**d**).

Figure 1b–d show the b_s field for $\alpha = D_s/D_m = 0.3$, $Pe = U_i d_p/D_m = 50$ and $k'' = 4$ in the three distinct cases, where d_p is the cylinder diameter. It is evident that the

shape of b_s is exactly the same in the three cases, but depending on the point at which the constraint $b_m = b_s = 0$ is enforced, the b_s field shifts towards positive or negative values. Consequently, since the H_s term is dominated by the contribution $-2k''U^x\langle b_s\rangle_{\Omega_s}/U_i$, the curves H_s vs. Pe are significantly affected by the point at which the constraint is imposed, and there is nothing to prevent it from also obtaining negative values, as in the case where the constraint is enforced in point 1.

This is confirmed by dispersion data reported in Figure 2 showing the behavior of $h_s = H_s/d_p$ vs. Pe in the three cases considered above, and the corresponding curves $h_m = H_m/d_p$ vs. Pe. Obviously, if h_s changes with the point of constraint, h_m also changes because their sum $h = H/d_p = h_m + h_s$ is not affected by the constraint point. This analysis clearly indicates that the identification of H_m and H_s based on Equation (14) cannot be adopted because it provides non-unique results, in contrast to the approach based on Equation (15), which instead allows for a unique decomposition of H into H_m^g and H_s^g that is independent of the constraint point. It is important to note, however, that although H_m^g and H_s^g allow for a unique decomposition of the contributions of the moving zone and the stationary zone, this does not imply that the two terms are independent since the b-fields are intrinsically interdependent via the boundary conditions, Equations (11) and (12). This mutual dependence underlies the limitations of the Giddings' approach, as will be shown in Section 3.2.

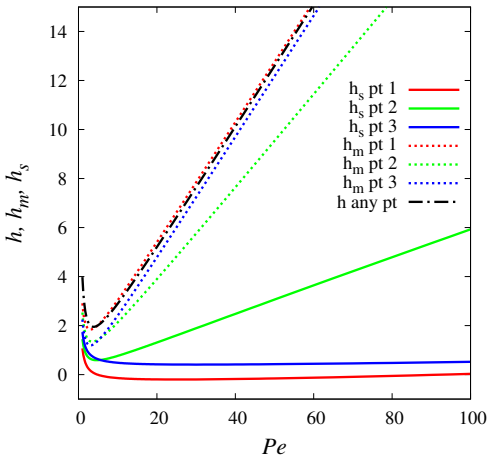


Figure 2. Normalized total plate height $h = H/d_p$ vs. $Pe = U_i d_p/D_m$ (black dot–dashed curve) of the square array of fully porous cylinders for $\alpha = D_s/D_m = 0.3$, $k'' = 4$, and the three different splits in $h_m = H_m/d_p$ and $h_s = H_s/d_p$ depending on the point at which the constraint $b_m = b_s = 0$ is enforced.

3.2. Identification of H_{Cm} and H_{Cs}

To isolate H_{Cm} and H_{Cs} from H, we first need to determine the H_B contribution, to subsequently subtract it from H. By setting the eluent velocity field to zero in Equations (9) and (10), $\mathbf{v} = \mathbf{0}$, that implies $v_x = 0$, $U_i = 0$ and $U^x = 0$, the b-fields $b_m^0 = b_m|_{\mathbf{v}=\mathbf{0}}$ and $b_m^0 = b_m|_{\mathbf{v}=\mathbf{0}}$, satisfy the diffusion equations

$$D_m\nabla^2 b_m^0 = 0 \quad (16)$$

$$D_s\nabla^2 b_s^0 = 0 \quad (17)$$

and boundary conditions of Equations (11)–(13). The two fields b_m^0 and b_s^0 allow for the estimate of the B term H_B via the simplified form of Equations (14) and (15):

$$H_B = H_{Bm} + H_{Bs} = \underbrace{\frac{2D_m}{U_i}\left(1 - \langle \partial_x b_m^0 \rangle_{\Omega_m}\right)}_{H_{Bm}} + \underbrace{\frac{2D_s k''}{U_i}\left(1 - \langle \partial_x b_s^0 \rangle_{\Omega_s}\right)}_{H_{Bs}} \tag{18}$$

or equivalently

$$H_B = H_{Bm}^g + H_{Bs}^g = \underbrace{\frac{2D_m}{U_i}\left\langle ||\nabla b_m^0 - \mathbf{e}_x||^2 \right\rangle_{\Omega_m}}_{H_{Bm}^g} + \underbrace{\frac{2D_s\, k''}{U_i}\left\langle ||\nabla b_s^0 - \mathbf{e}_x||^2 \right\rangle_{\Omega_s}}_{H_{Bs}^g} \tag{19}$$

Also in this case, Equations (18) and (19) are fully equivalent, meaning that they furnish exactly the same result in terms of H_B but allow for a different decomposition of the two contributions of the mobile and stationary zones, i.e., $H_{Bm} + H_{Bs} = H_{Bm}^g + H_{Bs}^g$ but $H_{Bm} \neq H_{Bm}^g$ and $H_{Bs} \neq H_{Bs}^g$.

The two different formulations of H and H_B lead to the same H_C term but to different splits of the two contributions H_{Cm} and H_{Cs}. Indeed, from Equations (14) and (18), one obtains

$$\begin{aligned} H_C = H - H_B = \underbrace{(H_m - H_{Bm})}_{H_{Cm}} + \underbrace{(H_s - H_{Bs})}_{H_{Cs}} = \\ \underbrace{\frac{2D_m}{U_i}\left(\langle \partial_x b_m^0 - \partial_x b_m \rangle_{\Omega_m}\right) + \frac{2}{U_i}\left\langle (v_x - U^x)\, b_m \right\rangle_{\Omega_m}}_{H_{Cm}} \\ + \underbrace{\overbrace{\frac{2D_s k''}{U_i}\left(\langle \partial_x b_s^0 - \partial_x b_s \rangle_{\Omega_s}\right)}^{H_{Cs1}} - \overbrace{\frac{2k'' U^x}{U_i}\left\langle b_s \right\rangle_{\Omega_s}}^{H_{Cs2}}}_{H_{Cs}} \end{aligned} \tag{20}$$

whereas from Equations (15) and (19), one obtains

$$\begin{aligned} H_C = H - H_B = \underbrace{(H_m^g - H_{Bm}^g)}_{H_{Cm}^g} + \underbrace{(H_s^g - H_{Bs}^g)}_{H_{Cs}^g} = \\ \underbrace{\frac{2D_m}{U_i}\left\langle ||\nabla b_m - \mathbf{e}_x||^2 - ||\nabla b_m^0 - \mathbf{e}_x||^2 \right\rangle_{\Omega_m}}_{H_{Cm}^g} + \\ \underbrace{\frac{2D_s\, k''}{U_i}\left\langle ||\nabla b_s - \mathbf{e}_x||^2 - ||\nabla b_s^0 - \mathbf{e}_x||^2 \right\rangle_{\Omega_s}}_{H_{Cs}^g} \end{aligned} \tag{21}$$

The identification of H_{Cm} and H_{Cs} based on Equation (20) suffers from the same drawback as Equation (14), that is, it is not unique and depends on the point of constraint, unlike the formulation based on Equation (21), which is instead unique and independent of the point of constraint. Nevertheless, it is interesting to analyze Equation (20) in detail because it allows us to highlight the limitations and flaws of Giddings' approach to the H_{Cs} term.

3.3. Limitations and Flaws of Giddings' Approach

The Giddings' Equation (3) for the H_{Cs} term requires the estimate of the shape factor q_f, defined as $q_f = 2\langle\theta\rangle_{\Omega_s}$, θ being a dimensionless field, defined in the stationary zone Ω_s, satisfying the following Poisson equation and boundary conditions:

$$\nabla^2\theta = -1/L_r^2 \quad (22)$$

$$\theta|_{\partial\Omega_s} = 0 \quad (23)$$

$$\nabla\theta\cdot\mathbf{n}|_{\partial\Omega_s^{\text{imp}}} = 0 \quad (24)$$

where L_r is a reference length, usually the particle radius or the pillar radius $L_r = R_p = d_p/2$ for the packing of spheres or pillar array columns. The analytical solutions of Equations (22)–(24) for fully porous or porous-shell spherical and cylindrical particles are reported in Appendix B, together with the corresponding values of the shape factor q_f. The boundary condition Equation (23) at the interface $\partial\Omega_s$ implies that the shape factor is totally independent of the transport process occurring in the mobile zone.

By comparing Equations (22) and (24) for θ with Equations (10) and (13) for b_s, it can be readily observed that b_s and θ are linearly related as

$$b_s = -\frac{L_r^2 U^x}{D_s}\theta + (x - x_0), \quad x_0 = \langle x\rangle_{\Omega_s} \quad (25)$$

By replacing Equation (25) for b_s into Equation (20), one obtains that the H_{Cs2} term attains the form

$$H_{Cs2} = -\frac{2k''U^x}{U_i}\langle b_s\rangle_{\Omega_s} = \frac{2k''U^x}{U_i}\frac{L_r^2 U_x}{D_s}\langle\theta\rangle_{\Omega_s} = \underbrace{2\langle\theta\rangle_{\Omega_s}}_{q_f}\frac{k''}{(1+k'')^2}\frac{L_r^2}{D_s}U_i \quad (26)$$

that coincides with Equation (3) for the H_{Cs} term proposed by Giddings, by setting $L_r = d_p/2$ as reference length. This observation, which highlights the strong similarities between the θ field and the b_s field, also allows us to point out the flaws in Giddings' approach, namely the following:

1. The H_{Cs1} term, which must sum in Equation (20) with the H_{Cs2} term in order to complete the H_{Cs} contribution of the stationary zone, is missing in Giddings' expression, Equation (3). The term H_{Cs1} plays a crucial role at low/intermediate Peclet values, and is absent only for axially invariant systems, for which b_m and b_s are independent of the axial coordinate x.
2. According to Equation (25), the boundary condition enforcing $\theta = 0$ at the whole boundary $\partial\Omega_s$, implies $b_s|_{\partial\Omega_s} = (x - x_0)|_{\partial\Omega_s}$, and therefore, is a very crude approximation of the actual boundary condition $b_s|_{\partial\Omega_s} = b_m|_{\partial\Omega_s}$, which properly accounts for the interaction between the mobile and stationary zones.

Figure 3 shows the θ field $\theta = (1 - (r/R_p)^2)/4$ and the analytical solution of the Giddings' Equation (22) with the boundary condition $\theta|_{\partial\Omega_s} = 0$ for the square array of fully porous cylinders, which is the same geometry analyzed in Figures 1 and 2. For comparison, Figure 3 b_m show the θ field—henceforth referred to as θ_{TZ}, evaluated from Equation (25) and the b_s field—solution of the transport scheme Equations (9)–(12), thus enforcing the proper boundary condition $b_s|_{\partial\Omega_s} = b_m|_{\partial\Omega_s}$. It can be observed that, for a very low value of the ratio $\alpha = D_s/D_m$, θ and θ_{TZ} are very similar. However, huge differences emerge for the highest value of α, namely $\alpha = 0.1$, throughout the range of Peclet values of practical interest, $Pe \in [10, 200]$. The higher the α value, usually in the range $\alpha \in [0.1, 0, 5]$ for silica columns [39], the greater the inaccuracy of the Giddings' prediction of the H_{Cs} term.

The inaccuracy is even larger if porous-shell particles are considered, as shown in Figure 4, where the comparison between θ (gray surface, Equation (A1)), and θ_{TZ} (colored surface) is shown in the case of a square array of porous-shell cylindrical particles (Figure 4a), where the ratio $\rho = R_i/R_p$ between the radius R_i of the impermeable core and the particle radius R_p is set to $\rho = 0.7$. For an easy comparison between θ and θ_{TZ} surfaces, the constraint point in the solution of the b_s field has been chosen in such a way that $\langle\theta\rangle_{\Omega_s} = \langle\theta_{TZ}\rangle_{\Omega_s}$.

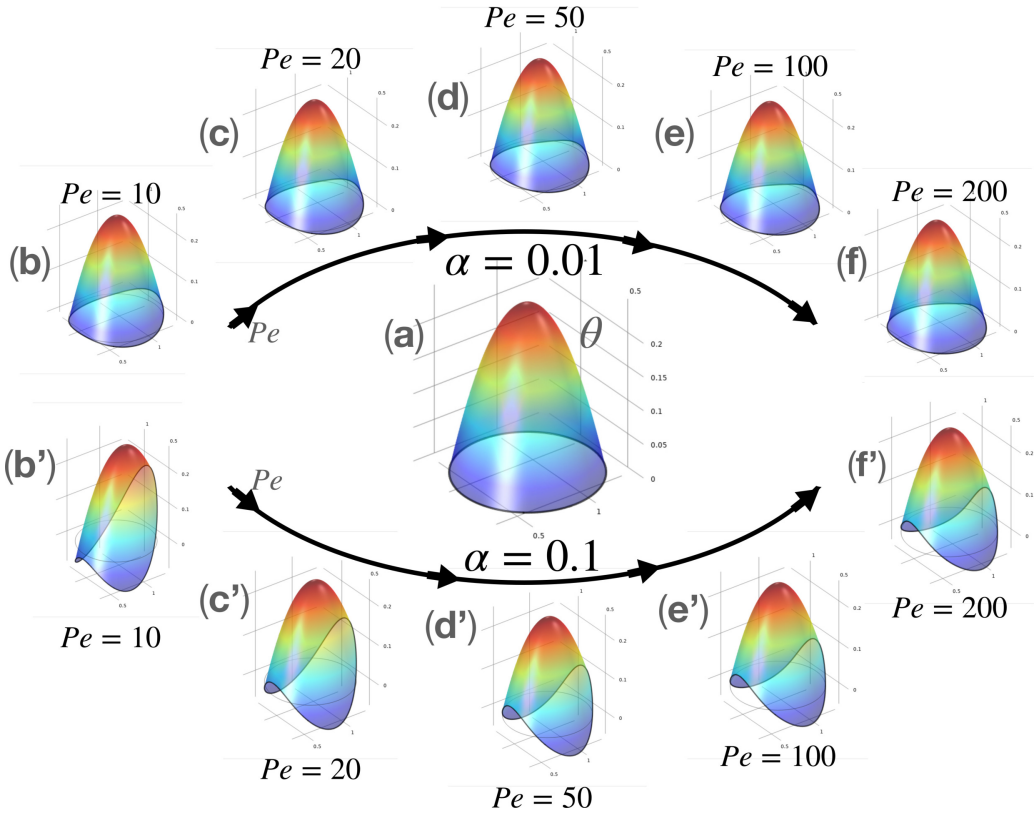


Figure 3. (**a**) θ evaluated from Giddings' equations, Equations (22) and (23). (**b**–**f'**) θ_{TZ} evaluated from Equation (25) and the b_s field, Equations (9)–(12), thus enforcing the proper boundary condition $b_s|_{\partial\Omega_s} = b_m|_{\partial\Omega_s}$. (**b**–**f**) refer to $\alpha = D_s/D_m = 0.01$. (**b'**–**f'**) refer to $\alpha = D_s/D_m = 0.1$.

3.4. The Gradient-Based Approach to H_{Cm} and H_{Cs}

In Section 3.2, we proposed to identify the terms H_{Cm} and H_{Cs} on the basis of Equation (21), i.e., through the use of the gradient-based H^g_{Cs} and H^g_{Cm} terms, because they are uniquely defined (independent of the constraint point) and account for the interplay between mass transfer in the mobile and stationary zones. In this section, we analyze in detail the numerical results for $H_{Cs} \equiv H^g_{Cs}$ and $H_{Cm} \equiv H^g_{Cm}$ for three different geometries, namely the 2D triangular array of cylinders (typical configuration of pillar array columns [4,22,23]), the 2D array of rectangular pillars (typical configuration of radially elongated pillar array columns [5,6]) and the 3D face-centered cubic array of spheres.

These three systems, shown in Figure 5, are investigated for the case of fully porous and porous-shell particles.

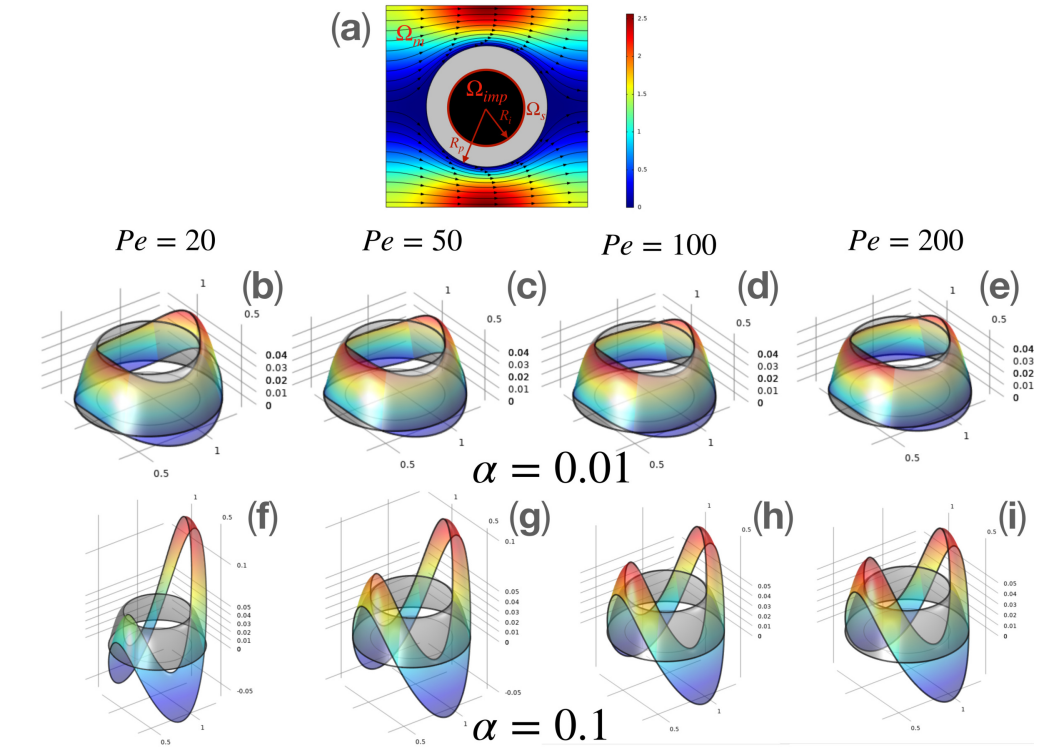


Figure 4. (**a**) Geometry of the square array of porous-shell cylindrical particles, $\rho = R_i/R_p = 0.7$. (**b**–**i**) Comparison between θ evaluated from Giddings equations, Equations (22) and (23) (gray surfaces), and θ_{TZ} (colored surfaces) evaluated from Equation (25) and the b_s field, Equations (9)–(13). (**b**–**e**) refer to $\alpha = D_s/D_m = 0.01$. (**f**–**i**) refer to $\alpha = D_s/D_m = 0.1$.

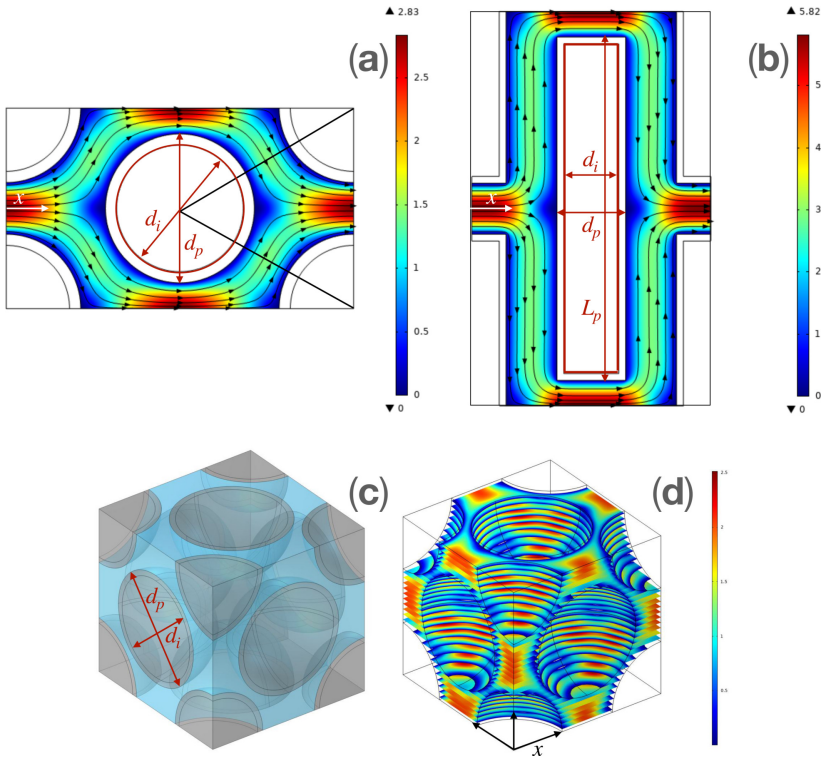


Figure 5. The 2D and 3D geometries investigated. (**a**) Array of 2D cylindrical pillars arranged on an equilateral triangular mesh, $\varepsilon = 0.5$ (**b**) Array of 2D rectangular pillars, aspect ratio $L_p/d_p = 5$, $\varepsilon = 0.5$. (**c**,**d**) Face-centered cubic array of spheres, $\varepsilon = 0.4$. Color plots indicate the intensity I of the normalized velocity field $I = ||\mathbf{v}||/U_i$. Arrow plots indicate the streamlines.

Figure 6a–f show the comparison of H_{Cs} vs. Pe curves, obtained by the TZMA approach, Equation (21), and Giddings' expression Equation (3), for the 2D triangular array of cylinders. It can be observed that for fully porous particles, there is a general agreement between the two results. Significant deviations are observed only for high values of α and high values of k''. On the contrary, for porous-shell particles, Giddings' expression significantly underestimates the H_{Cs} contribution, which actually strongly deviates from the linear behavior predicted via Equation (3). The inaccuracy of Giddings' predictions is even larger for the 2D array of rectangular pillars, as shown in Figure 7a–d. For rectangular pillars, with aspect ratio $L_p/d_p = 5$, the shape factor q_f has been numerically evaluated by solving Equations (22)–(24), thus obtaining $q_f = 0.562$ for fully porous pillars and $q_f = 0.062$ for porous-shell pillars with $\rho = 0.8$. Also for this system, the Giddings' approach tends to underestimate the H_{cs} term, especially for porous-shell particles and is unable to describe the non-monotonically increasing behavior of the H_{Cs} vs. Pe curves, which is particularly evident for porous-shell particles for low/intermediate values of Pe, as highlighted in Figure 7a'–d'. In general, all the curves H_{Cs} vs. Pe, for porous-shell particles, exhibit a strong nonlinear behavior that cannot be described by Equation (3), which postulates that H_{Cs} is a linear function of Pe.

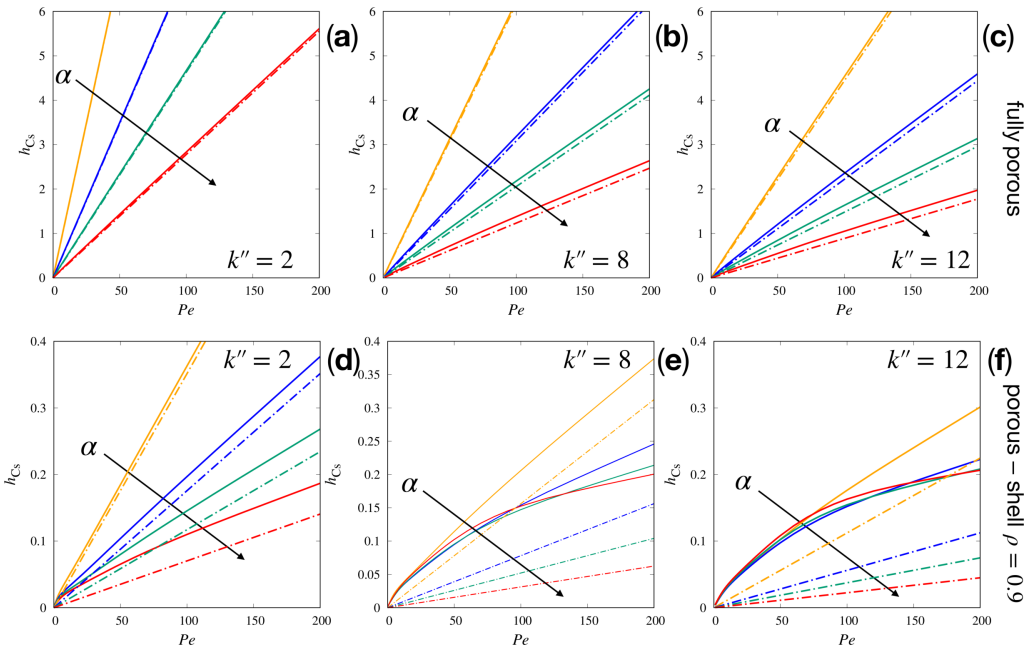


Figure 6. $h_{Cs} = H_{Cs}/d_p$ vs. $Pe = U_i d_p/D_m$ for the array of 2D cylindrical pillars, for fully porous particles (**a**–**c**) and porous-shell particles (**d**–**f**) with $\rho = d_i/d_p = 0.9$. Arrows indicate increasing values of $\alpha = D_s/D_m = 0.1$ (*orange*), 0.2 (*blue*), 0.3 (*green*), 0.5 (*red*). Three different values of k'' have been considered, namely $k'' = 2, 8, 12$. Continuous lines indicate results from the TZMA approach (Equation (21)). Dot–dashed lines indicate results from the Giddings' approach (Equation (3)).

Since Equation (3) significantly underestimates the H_{Cs} term, consequently, the H_{Cm} term, estimated as $H_C - H_{Cs}$, comes to be overestimated with the Giddings' approach, as shown in Figure 8a,b for the 2D array of fully porous rectangular pillars and in Figure 9b–d for the face-centered cubic array of fully porous and porous-shell particles. The larger α and k'', the greater the inaccuracy of Giddings' predictions in the underestimation of H_{Cs} and the consequent overestimation, by difference, of the H_{Cm} term.

Large errors in the prediction of H_{Cs} via Giddings' expression Equation (3) for porous-shell particles are compensated by the fact that the mass transfer resistance in the shell-stationary zone is small with respect to that in the mobile zone, i.e., $H_{Cs} \ll H_{Cm}$. For this reason, the resulting error in the estimate of H_{Cm} is around 15% for both fully porous and

porous-shell particles for $Pe \in [10, 100]$. It becomes definitely larger than 20% if larger values of Pe are considered, i.e., $Pe > 100$.

The remarkable inaccuracy of Giddings' predictions concerning the term H_{Cs} is due not only to the boundary condition $\theta|_{\partial\Omega_s} = 0$ but also to the absence of the term H_{Cs1}, as discussed in Section 3.3. The H_{Cs1} contributions is strictly zero for axially invariant systems. Indeed, when considering an axially invariant system, as the pillar array columns shown in Figure 10a, for which the main fluid flow component v_x is parallel to the pillar's symmetry axis, Giddings' expression for H_{Cs} is much more reliable in a wide range of α and k'' values, even for porous-shell particles, as shown in Figure 10b. This confirms that the inaccuracy of Giddings' predictions, for non-axially invariant systems, is due not only to the inexact boundary condition, which eliminates the coupling between zones, but also to the absence of the H_{Cs1} term.

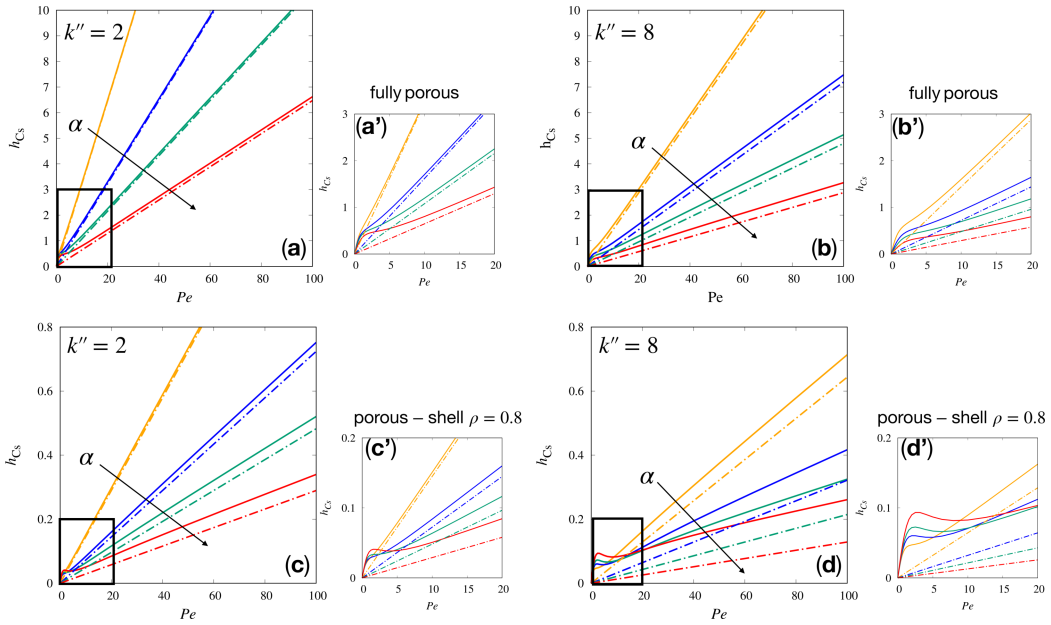


Figure 7. $h_{Cs} = H_{Cs}/d_p$ vs. $Pe = U_i d_p/D_m$ for the array of rectangular pillars, for fully porous particles (**a**,**b**) and porous-shell particles (**c**,**d**) with $\rho = d_i/d_p = 0.8$. Arrows indicate increasing values of $\alpha = D_s/D_m = 0.1$ (*orange*), 0.2 (*blue*), 0.3 (*green*), 0.5 (*red*). Two different values of k'' have been considered, namely $k'' = 2, 8$. (**a′**–**d′**) show the magnification of the corresponding (**a**–**d**) for $Pe \in [0, 20]$. Continuous lines indicate results from the TZMA approach (Equation (21)). Dotted lines indicate results from Giddings' approach (Equation (3)).

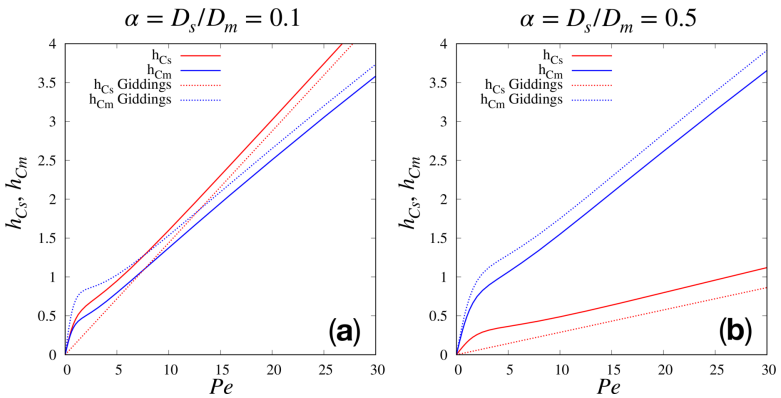


Figure 8. $h_{Cs} = H_{Cs}/d_p$ and $h_{Cm} = H_{Cm}/d_p$ vs. $Pe = U_i d_p/D_m$ for the array of fully porous rectangular pillars, for $k'' = 8$. (**a**) $\alpha = 0.1$. (**b**) $\alpha = 0.5$. Continuous lines indicate results from the TZMA approach (Equation (21)). Dot–dashed lines indicate results from the Giddings' approach (Equation (3)).

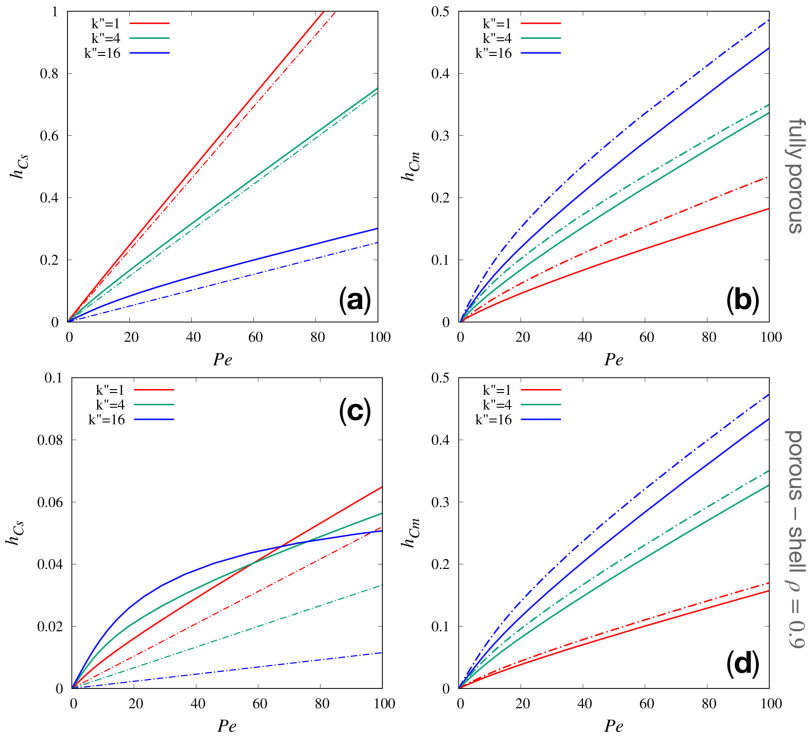


Figure 9. $h_{Cs} = H_{Cs}/d_p$ and $h_{Cm} = H_{Cm}/d_p$ vs. $Pe = U_i d_p/D_m$ for the face-centered cubic array of spheres, for $\varepsilon = 0.4$ and $\alpha = 0.3$. (**a**,**b**) Fully porous particles. (**c**,**d**) Porous-shell particles, $\rho = d_i/d_p = 0.9$. Three different values of k'' have been considered, namely $k'' = 1, 4, 16$. Continuous lines indicate results from the TZMA approach (Equation (21)). Dot–dashed lines indicate results from the Giddings' approach (Equation (3)).

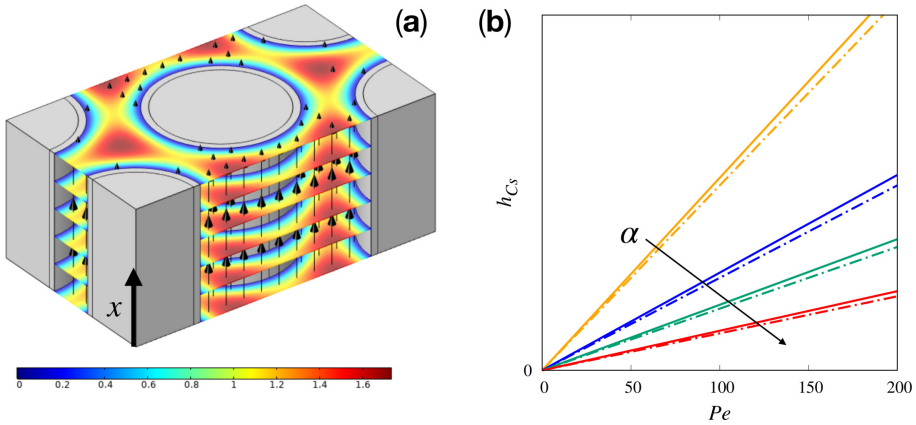


Figure 10. (**a**) Axially invariant system with the main fluid flow component v_x parallel to the pillar symmetry axis. Colors indicate the normalized axial velocity v_x/U_i. Arrows indicate the streamlines (straight lines). (**b**) $h_{Cs} = H_{Cs}/d_p$ vs. $Pe = U_i d_p/D_m$ for porous-shell pillars, $\rho = 0.9$ and $k'' = 8$. Arrow indicates increasing values of $\alpha = D_s/D_m = 0.1$ $(orange)$, $0.2(blue)$, 0.3 $(green)$, 0.5 (red).

4. Conclusions

A refined approach using the Two-Zone Moment Analysis (TZMA) method is introduced to assess the contributions of the mobile and stationary zones, H_{Cm} and H_{Cs}, to the van Deemter equation's H_C term. Two different formulations of H_{Cm} and H_{Cs} emerge from this method, offering different decompositions of H_C. The first formulation offers an expression for H_{Cs} that has similarities with, yet also significant differences from, the widely used Giddings' approach. While it addresses the limitation of Giddings' formulation (which assumes complete decoupling of the moving and stationary zones), the first formulation lacks uniqueness in the decomposition of H_C. On the other hand, the second formulation

captures the interaction between the two zones and provides a unique decomposition. The latter is the one we propose to investigate and quantify the contributions of the mobile and stationary zones to the total plate height.

Three geometries were examined: the 2D triangular array of cylinders, the 2D rectangular pillar array and the 3D face-centered cubic array of spheres. Numerical data for H_{Cs} versus Pe curves for these geometries demonstrate that while Giddings' approach generally matches results for fully porous particles, it significantly underestimates H_{Cs} for porous-shell particles, particularly at higher values of α and k''. For porous-shell particles, Giddings' method fails to capture the nonlinear H_{Cs} versus Pe behavior, as it assumes a linear relationship.

Since Giddings' expression underestimates H_{Cs}, the H_{Cm} term (calculated as $H_C - H_{Cs}$) is overestimated, with the discrepancies increasing as α and k'' rise. The errors in predicting H_{Cs} for porous-shell particles are compensated by the low mass transfer resistance in the shell-stationary zone, leading to low accuracy in the prediction of H_{Cm} that is quantifiable with an error of around 15% for $Pe \in [10, 100]$, and >20% for $Pe > 100$, and is comparable in the fully porous and the porous-shell case.

The inaccuracies in Giddings' predictions arise not only from boundary conditions, but also from the absence of the H_{Cs1} term, which is zero in axially invariant systems. For the latter, Giddings' expression for H_{Cs} is more reliable across a wider range of α and k'' values, even for porous-shell particles.

Author Contributions: Conceptualization, A.A. and G.D.; methodology, A.A. and G.D.; software, A.A.; validation, A.A.; formal analysis, A.A. and G.D.; investigation, A.A. and G.D.; resources, A.A.; data curation, A.A.; writing—original draft preparation, A.A.; writing—review and editing, A.A. and G.D.; visualization, A.A. and G.D.; supervision, A.A. and G.D.; project administration, A.A.; funding acquisition, A.A. All authors have read and agreed to the published version of this manuscript.

Funding: Research was funded by ICSC CN1 Spoke 6.

Data Availability Statement: Data are available from the corresponding author upon request.

Conflicts of Interest: The authors declare no conflicts of interest.

Appendix A

Numerical results for the velocity field **v** and the b-fields b_m and b_s were obtained through the solution of their respective partial differential equations using Comsol Multiphysics 5.5 that employs the Finite Element Method. The incompressible Navier–Stokes package (Stokes flow) was adopted under stationary conditions, utilizing P2 + P1 Lagrange elements for velocity and pressure, respectively. For the numerical integration of the coupled stationary transport equations of b_m and b_s, the Coefficient Form Partial Differential Equation (PDE) package was utilized with Lagrangian quadratic elements. The Multifrontal Massively Parallel Sparse direct Solver (MUMPS) linear solver was employed with a relative tolerance of 10^{-6}. The complete triangular mesh of 2D geometries consisted of approximately 1×10^5 domain elements, 1×10^4 boundary elements, and 4×10^2 edge elements. The complete tetrahedral mesh of the 3D geometry consisted of approximately 2×10^6 domain elements, 2×10^5 boundary elements, and 2×10^3 edge elements. Results were verified to be mesh-independent in the whole range of investigated Pe values, $Pe \in (10^{-2}, 200)$.

Appendix B

The analytical solution of Equations (22)–(24) for 2D cylindrical shell particles reads as

$$\theta(\widetilde{r}) = (1 - \widetilde{r}^2 + 2\rho^2 \log \widetilde{r})/4, \quad \widetilde{r} = r/R_p, \quad \rho = R_i/R_p \tag{A1}$$

where R_i is the impermeable core radius and R_p the particle radius. The shape factor $q_f = 2\langle\theta\rangle_{\Omega_s}$ attains the form

$$q_f = \frac{1}{4} - \frac{3\rho^2}{4} - \frac{\rho^4 \log\rho}{1-\rho^2} \tag{A2}$$

The corresponding equations for 2D fully porous cylindrical particles are obtained from Equations (A1) and (A2) by taking the limit $\rho \to 0$.

The analytical solution of Equations (22)–(24) for 3D spherical shell particles reads as

$$\theta(\widetilde{r}) = \frac{(-2\rho^3 + \widetilde{r} + 2\rho^3\widetilde{r} - \widetilde{r}^3)}{6\widetilde{r}} \tag{A3}$$

The shape factor q_f attains the form

$$q_f = \frac{2}{15}\frac{(-1+\rho)^2(1+3\rho+6\rho^2+5\rho^3)}{1+\rho+\rho^2} \tag{A4}$$

The corresponding equations for 3D fully porous spherical particles are obtained from Equations (A3) and (A4) by setting $\rho = 0$.

References

1. Sarwar, M.S.; Simon, U.; Dimartino, S. Experimental investigation and mass transfer modelling of 3D printed monolithic cation exchangers. *J. Chromatogr. A* **2021**, *1646*, 462125. [CrossRef]
2. Conti, M.; Boland, D.; Heeran, C.; Symington, J.A.; Pullen, J.R.; Dimartino, S. Purification of monoclonal antibodies using novel 3D printed ordered stationary phases. *J. Chromatogr. A* **2024**, *1722*, 464873. [CrossRef] [PubMed]
3. Feast, S.; Titterington, J.; Hoang, V.A.; Allison, T.M.; Fee, C.; Nazmi, A.R. Purification of his-tagged proteins using printed monolith adsorption columns. *J. Chromatogr. A* **2024**, *1733*, 465216. [CrossRef]
4. Malsche, W.D.; Gardeniers, H.; Desmet, G. Experimental Study of Porous Silicon Shell Pillars under Retentive Conditions. *Anal. Chem.* **2008**, *80*, 5391–5400 . [CrossRef] [PubMed]
5. Broeckhoven, K.; Desmet, G. Advances and Innovations in Liquid Chromatography Stationary Phase Supports. *Anal. Chem.* **2021**, *93*, 257–272. [CrossRef] [PubMed]
6. Vankeerberghen, B.; Op de Beeck, J.; Desmet, G. Column-Only Band Broadening in a Porous Shell Radially Elongated Pillar Array Column. *Anal. Chem.* **2024**, *96*, 3618–3626. [CrossRef] [PubMed]
7. Desmet, G.; Broeckhoven, K. Equivalence of the Different Cm- and Cs-Term Expressions Used in Liquid Chromatography and a Geometrical Model Uniting Them. *Anal. Chem.* **2008**, *80*, 8076–8088. [CrossRef] [PubMed]
8. Gritti, F.; Guiochon, G. The van Deemter equation: Assumptions, limits, and adjustment to modern high performance liquid chromatography. *J. Chromatogr. A* **2013**, *1302*, 1–13. [CrossRef]
9. Knox, J.H. Band dispersion in chromatography—A universal expression for the contribution from the mobile zone. *J. Chromatogr. A* **2002**, *960*, 7–18. [CrossRef] [PubMed]
10. Miyabe, K.; Matsumoto, Y.; Guiochon, G. Peak Parking-Moment Analysis. A Strategy for the Study of the Mass-Transfer Kinetics in the Stationary Phase. *Anal. Chem.* **2007**, *79*, 1970–1982. [CrossRef] [PubMed]
11. Miyabe, K.; Ando, N.; Guiochon, G. Peak parking method for measurement of molecular diffusivity in liquid phase systems. *J. Chromatogr. A* **2009**, *1216*, 4377–4382. [CrossRef]
12. Miyabe, K.; Nagai, J.i.; Guiochon, G. Peak parking-moment analysis: A strategy for the measurement of molecular diffusivity in liquid phase. *Chem. Eng. Sci.* **2010**, *65*, 3859–3864. [CrossRef]
13. Desmet, G.; Deridder, S. Effective medium theory expressions for the effective diffusion in chromatographic beds filled with porous, non-porous and porous-shell particles and cylinders. Part I: Theory. *J. Chromatogr. A* **2011**, *1218*, 32–45. [CrossRef] [PubMed]
14. Hlushkou, D.; Liasneuski, H.; Tallarek, U.; Torquato, S. Effective diffusion coefficients in random packings of polydisperse hard spheres from two-point and three-point correlation functions. *J. Appl. Phys.* **2015**, *118*, 124901. [CrossRef]
15. Adrover, A.; Venditti, C.; Desmet, G. An alternative general model for the effective longitudinal diffusion in chromatographic beds filled with ordered porous particles. *J. Chromatogr. A* **2024**, *1715*, 464598. [CrossRef] [PubMed]
16. Adrover, A.; Venditti, C.; Desmet, G. On the modelling of the effective longitudinal diffusion in bi-continuous chromatographic beds. *J. Chromatogr. A* **2024**, *1721*, 464817. [CrossRef] [PubMed]
17. Giddings, J.C. *Dynamics of Chromatography: Principles and Theory*; CRC Press: Boca Raton, FL, USA, 2017.

18. Gritti, F.; Guiochon, G. General HETP equation for the study of mass-transfer mechanisms in RPLC. *Anal. Chem.* **2006**, *78*, 5329–5347. [CrossRef]
19. De Wilde, D.; Detobel, F.; Billen, J.; Deconinck, J.; Desmet, G. Modelling the relation between the species retention factor and the C-term band broadening in pressure-driven and electrically driven flows through perfectly ordered 2-D chromatographic media. *J. Sep. Sci.* **2009**, *32*, 4077–4088. [CrossRef]
20. Matheuse, F.; Deridder, S.; Desmet, G. An explicit expression for the retention factor and velocity dependency of the mobile zone mass transfer band broadening in packed spheres beds used in liquid chromatography. *J. Chromatogr. A* **2020**, *1634*, 461710. [CrossRef]
21. Huygens, B.; Venditti, C.; Adrover, A.; Desmet, G. Nonadditivity and Nonlinearity of Mobile and Stationary Zone Mass Transfer Resistances in Chromatography. *Anal. Chem.* **2023**, *95*, 15199–15207. [CrossRef] [PubMed]
22. Moussa, A.; Huygens, B.; Venditti, C.; Adrover, A.; Desmet, G. Theoretical computation of the band broadening in micro-pillar array columns. *J. Chromatogr. A* **2024**, *1715*, 464607. [CrossRef]
23. Moussa, A.; Huygens, B.; Venditti, C.; Adrover, A.; Desmet, G. On the contribution of the top and bottom walls in micro-pillar array columns and related high-aspect ratio chromatography systems. *J. Chromatogr. A* **2024**, *1720*, 464825. [CrossRef] [PubMed]
24. Venditti, C.; Giona, M.; Adrover, A. Exact moment analysis of transient/asymptotic dispersion properties in periodic media with adsorbing/desorbing walls. *Phys. Fluids* **2022**, *34*. [CrossRef]
25. Venditti, C.; Huygens, B.; Desmet, G.; Adrover, A. Moment analysis for predicting effective transport properties in hierarchical retentive porous media. *J. Chromatogr. A* **2023**, *1703*, 464099. [CrossRef] [PubMed]
26. Lauriola, C.; Venditti, C.; Desmet, G.; Adrover, A. Dispersion properties of triply periodic minimal surface stationary phases for LC: The case of superficial adsorption. *J. Chromatogr. A* **2025**, *1743*, 465676. [CrossRef] [PubMed]
27. Brenner, H.; Edwards, D.A. *Macrotransport Processes*; Butterworth-Heinemann: London, UK, 1993.
28. Brenner, H.; Adler, P.M.; Stewartson, K. Dispersion resulting from flow through spatically periodic porous media II. Surface and intraparticle transport. *Philos. Trans. R. Soc. Lond. Ser. A Math. Phys. Sci.* **1982**, *307*, 149–200. [CrossRef]
29. Yan, X.; Wang, Q.; Bau, H.H. Dispersion in retentive pillar array columns. *J. Chromatogr. A* **2010**, *1217*, 1332–1342. [CrossRef] [PubMed]
30. Yan, X.; Wang, Q.; Li, N. Predictive model of solute transport with reversible adsorption in spatially periodic hierarchical porous media. *J. Chromatogr. A* **2015**, *1407*, 69–75. [CrossRef] [PubMed]
31. Schure, M.R.; Maier, R.S.; Kroll, D.M.; Davis, H.T. Simulation of packed-bed chromatography utilizing high-resolution flow fields: Comparison with models. *Anal. Chem.* **2002**, *74*, 6006–6016. [CrossRef]
32. Schure, M.R.; Maier, R.S.; Kroll, D.M.; Davis, H.T. Simulation of ordered packed beds in chromatography. *J. Chromatogr. A* **2004**, *1031*, 79–86. [CrossRef]
33. Ghosh, R.; Chen, G. Mathematical modelling and evaluation of performance of cuboid packed-bed devices for chromatographic separations. *J. Chromatogr. A* **2017**, *1515*, 138–145. [CrossRef] [PubMed]
34. Umatheva, U.; Chen, G.; Ghosh, R. Computational fluid dynamic (CFD) simulation of a cuboid packed-bed chromatography device. *Chem. Eng. Res. Des.* **2019**, *152*, 393–401. [CrossRef]
35. Xu, Y.; Umatheva, U.; Ghosh, R. Evaluation of a Novel Cuboid Hollow Fiber Hemodialyzer Design Using Computational Fluid Dynamics. *Membranes* **2023**, *13*, 93. [CrossRef]
36. Gritti, F.; Guiochon, G. Mass transfer kinetics, band broadening and column efficiency. *J. Chromatogr. A* **2012**, *1221*, 2–40. [CrossRef]
37. Cavazzini, A.; Gritti, F.; Kaczmarski, K.; Marchetti, N.; Guiochon, G. Mass-Transfer Kinetics in a Shell Packing Material for Chromatography. *Anal. Chem.* **2007**, *79*, 5972–5979. [CrossRef] [PubMed]
38. Horváth, K.; Gritti, F.; Fairchild, J.N.; Guiochon, G. On the optimization of the shell thickness of superficially porous particles. *J. Chromatogr. A* **2010**, *1217*, 6373–6381. [CrossRef] [PubMed]
39. Liekens, A.; Denayer, J.; Desmet, G. Experimental investigation of the difference in B-term dominated band broadening between fully porous and porous-shell particles for liquid chromatography using the Effective Medium Theory. *J. Chromatogr. A* **2011**, *1218*, 4406–4416. [CrossRef] [PubMed]

Disclaimer/Publisher's Note: The statements, opinions and data contained in all publications are solely those of the individual author(s) and contributor(s) and not of MDPI and/or the editor(s). MDPI and/or the editor(s) disclaim responsibility for any injury to people or property resulting from any ideas, methods, instructions or products referred to in the content.